Geophysical Research Letters®

Key Points:

- Banded chorus events typically have a more pronounced plateau shape than no-gap events in the parallel electron distribution
- The electron plateau can cause severe damping at $\sim 0.5 f_{ce}$ via cyclotron resonance, and roughly determine the gap frequency
- There is no significant difference between the normalized electron velocity distributions in banded and no-gap events

Unraveling the Role of Electron Plateau Distributions in the Power Gap Formation of Chorus Waves: Van Allen Probes Observations

Huayue Chen[1,2] [ID], **Rui Chen[1,3,4]** [ID], **Xinliang Gao[1,3,4]** [ID], **Quanming Lu[1,3,4]** [ID], **Yangguang Ke[1,3,4]** [ID], and **Zhenyu Kong[1,3,4]** [ID]

[1]Deep Space Exploration Laboratory, School of Earth and Space Sciences, University of Science and Technology of China, Hefei, China, [2]Department of Physics, Auburn University, Auburn, AL, USA, [3]CAS Center for Excellence in Comparative Planetology, Hefei, China, [4]Collaborative Innovation Center of Astronautical Science and Technology, Harbin, China

Abstract The power gap of chorus waves at $\sim 0.5 f_{ce}$ has been discovered for decades, but its generation mechanism is still under debate. Previous studies have revealed that electron plateau distributions are vitally important for the gap formation. By analyzing over one-year Van Allen Probes data, we have studied chorus waves with (banded events) and without a power gap (no-gap events), and their correlations with the electron plateau distribution. Although there is no significant difference in the morphology of velocity distributions in banded and no-gap events, banded chorus events are typically accompanied by a plateau component with about one order higher number density than no-gap events. The plateau components can cause severe damping at $\sim 0.5 f_{ce}$ through cyclotron resonance rather than Landau resonance, and the gap frequency is roughly determined by the bulk velocity of plateau components. Our study provides new observational constraints on the generation mechanisms of power gap.

Plain Language Summary The generation mechanism of power gap at $\sim 0.5 f_{ce}$ of chorus waves has been a long-standing problem for decades. Although its generation mechanism is still under debate, there is a consensus that the electron plateau in the parallel velocity distribution is a key factor to solve this problem. Here, we try to find out what role the electron plateau plays in the gap formation based on a statistical analysis of Van Allen Probes data. First of all, we find banded chorus events indeed have a more pronounced plateau shape (about one order higher number density) than no-gap events, confirming the importance of electron plateau. We further find that the electron plateau can cause the severe wave damping at $\sim 0.5 f_{ce}$ via cyclotron resonance rather than Landau resonance, and the gap frequency is roughly determined by the bulk velocity of electron plateau based on the cyclotron resonance condition. We also compare the morphology of electron velocity distributions in banded and no-gap events, but do not find an obvious difference between them. Our study provides new observational constraints on the generation mechanisms of the power gap, which may help scientists finally solve this problem.

1. Introduction

Chorus waves are intense and coherent whistler-mode emissions that naturally occur in the Earth's inner magnetosphere (Burtis & Helliwell, 1969; Horne & Thorne, 1998; Tsurutani & Smith, 1974), usually exhibiting as a series of repetitive elements in the time-frequency spectrum (Chen, Lu, et al., 2022; Gao et al., 2022; Lu et al., 2021). These waves are well-known for their significant influences on electron dynamics, such as accelerating ~ 100 keV electrons to relativistic energies (Meredith et al., 2001; Summers et al., 1998; Thorne et al., 2013), and scattering ~ 10 keV electrons to form the diffuse aurora or pulsating aurora (Kasahara et al., 2018; Nishimura et al., 2013). One of the typical characteristics of chorus waves is the power minimum around $0.5 f_{ce}$ (where f_{ce} is the equatorial electron gyrofrequency, Gao et al., 2019; Li et al., 2011; Teng et al., 2019; Tsurutani & Smith, 1974, 1977), known as the power gap. The gap naturally separates chorus waves into the lower band (0.1–$0.5 f_{ce}$) and upper band (0.5–$0.8 f_{ce}$), and such waves with a gap are called banded chorus waves. Both THEMIS and Van Allen Probes observations reveal that banded chorus waves are preferentially detected in their source region, that is, the magnetic equator (Gao et al., 2019; Teng et al., 2019).

Although the power gap has been discovered for more than 50 years (Tsurutani & Smith, 1974), the generation mechanism is still under debate. Omura et al. (2009) have proposed that the power gap can be caused by the

severe nonlinear Landau damping for the waves at $\sim 0.5 f_{ce}$ during the poleward propagation. The wave-wave coupling has also been introduced to explain the gap formation (Chen et al., 2017; Gao et al., 2016, 2017), where upper band waves appear as harmonic of lower band waves, and the gaps are naturally formed. However, both mechanisms are more suitable for the interpretation of banded chorus waves at higher latitudes where the waves become oblique.

Besides, there also exist two mechanisms to explain those banded chorus waves detected in the equatorial region. Li et al. (2019) suggested that the electron plateau distribution at $\sim 0.5 V_{Ae}$ (V_{Ae} is the electron Alfven speed) caused by the Landau resonance of whistler-mode waves can divide the entire electron velocity distribution into two parts, and then the two electron populations separately excite the lower band and upper band waves, leaving a power gap between them. Essentially the formation of the power gap is due to the separate growth of two bands of waves. This mechanism is developed from the previous studies by Liu et al. (2011) and Fu et al. (2014). However, Chen et al. (2021) and Chen, Gao, et al. (2022) have proposed that the power gap is caused by the severe damping of waves at $\sim 0.5\Omega_e$ rather than the separate excitation of different wave bands. By calculating the growth rate (see Figure 4 in Chen, Gao, et al., 2022), they have found that after the formation of electron plateau distribution, all the wave modes reach saturation and begin to decay, but the waves at $\sim 0.5 f_{ce}$ experience the most severe damping through the cyclotron resonance with the electron plateau component. They call this mechanism as "spectrum bite." Both mechanisms have pointed out the potential roles of electron plateau distribution in the formation of the power gap, but no observational support has been provided for either one.

In this study, we perform a statistical analysis of Van Allen Probes data to investigate the correlation of power gaps with the electron plateau distribution. The results show that the occurrence of power gaps relies on the number density of electron plateau distribution, and the frequency of power gaps can be roughly determined by the bulk velocity of electron plateau. This study can provide observational constraints to the existing mechanisms.

2. Van Allen Probes and Instrumentation

The Van Allen Probes are twin spacecraft operating in highly elliptical and near-equatorial orbits, with perigees below $2 R_E$ (R_E is the Earth radius) and apogees above $6 R_E$ (Kessel et al., 2012). The Electric and Magnetic Field Instrument Suite and Integrated Science (EMFISIS) can provide not only the high-resolution (35,000 samples/sec) waveform data with each segment lasting ~ 6 s, but also the low-resolution (64 samples/sec) triaxial magnetic field data (Kletzing et al., 2013). Here the low-resolution magnetic field is treated as the background magnetic field B_0, which is used to calculate the electron gyrofrequency. The electron distributions with a time resolution of ~ 22 s are provided by the Helium, Oxygen, Proton, and Electron (HOPE) Mass Spectrometer (Funsten et al., 2013), covering an energy range from 10 eV to 50 keV. The pitch angle (PA) = 18°, PA = 162°, and PA = 90° channels of the HOPE instrument are treated as the parallel, antiparallel and perpendicular directions. The plasma density n_0 is estimated from the upper hybrid frequency measured by the high frequency receiver (Kurth et al., 2015).

3. Observational Results

3.1. Example Events

Figure 1 shows two representative examples of chorus events, including the (a) magnetic spectrum density, (b) wave normal angle (WNA) θ, (c) Sz/S (where S is the Poynting flux and Sz is the parallel component). Event I (left column) is a banded event, which contains an obvious power gap at $\sim 0.5 f_{ce}$. While Event II (right column) has a continuous frequency band across $0.5 f_{ce}$, called "no-gap event" hereafter. In all panels, the dashed lines in white or black denote $0.5 f_{ce}$. Both events are quasi-parallel propagating ($\theta < 30°$), but their propagating directions are different: Event I is along the magnetic field line (Sz/S ≈ 1), while Event II is opposite to it (Sz/S ≈ -1).

The phase space densities (PSDs) of electrons as a function of the parallel velocity $v_{\parallel}/V_{Ae}$ ($V_{Ae} = B_0/\sqrt{\mu_0 n_0 m_e}$, μ_0 is the permeability of vacuum, and m_e is the electron mass) for Events I and II are denoted by black dots in Figures 1d–1g. The PSDs (d, f) along the wave propagation ($\vec{k}$) and (e, g) opposite to it are separately displayed, and are selected during each chorus event, that is, a 6-s segment. However, if no HOPE data is falling within the 6-s segment, then we use the closest data point before this segment. In either direction of each event, the PSD contains an obvious plateau shape at $v_{\parallel}/V_{Ae} \sim 0.5$.
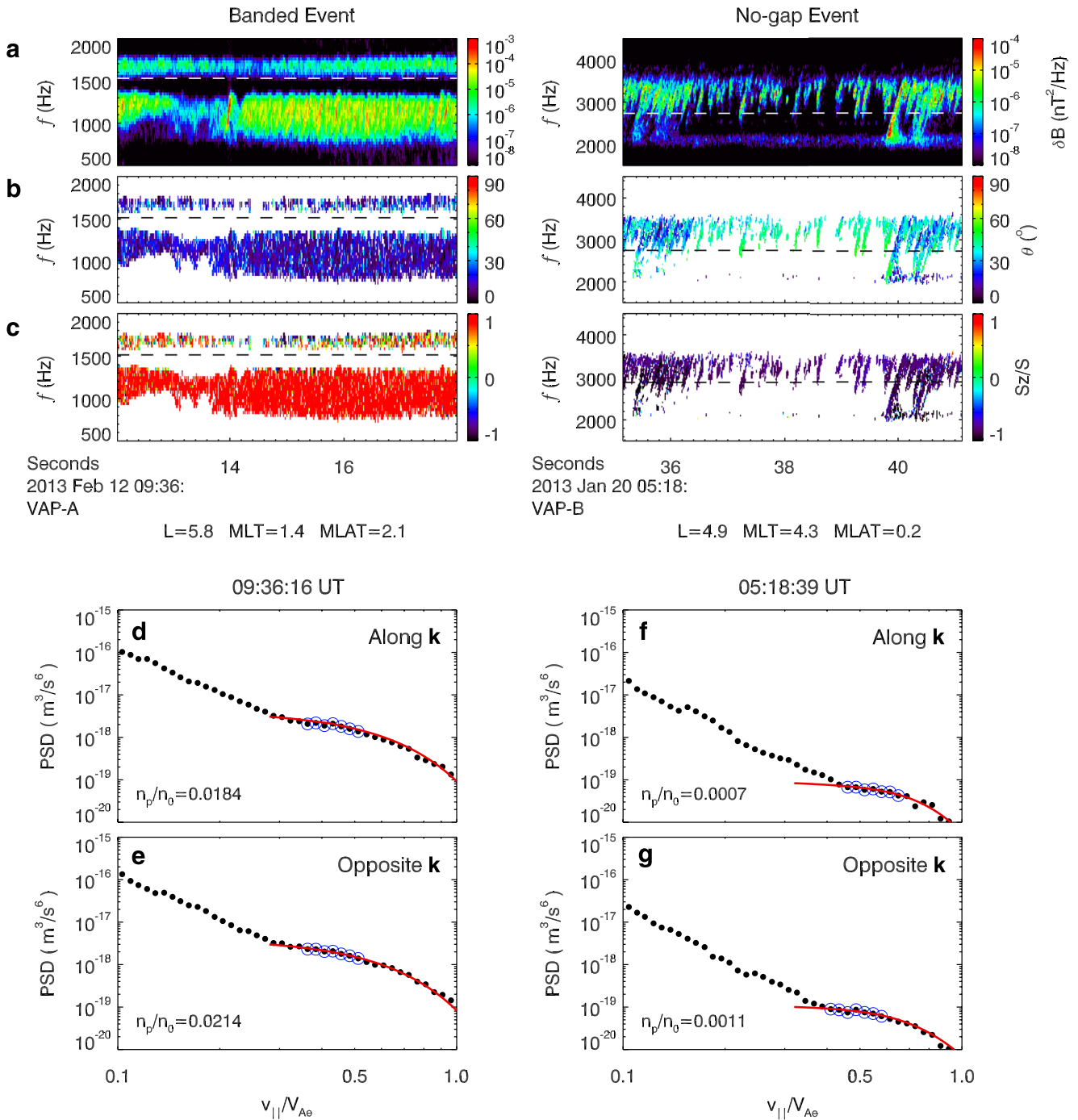
Figure 1. (a) The magnetic spectrogram, (b) wave normal angle θ, and (c) ratio Sz/S in Event I (left column) and Event II (right column). The dashed lines in white or black denote $0.5f_{ce}$. The phase space densities (d, f) along and (e, g) opposite to the wave propagation ($\vec{k}$) in Event I and in Event II. The black dots are detected values, and seven of them marked by blue cycles are chosen to perform fitting, with the fitting distributions represented by red lines.

To estimate the number density of these plateau components, we assume the velocity distribution $f_\parallel$ as the combination of a hot component and a plateau component:

$$f_\parallel = n_h \left(\pi v_{th\parallel,h}^2 \right)^{-\frac{1}{2}} \exp\left(-\frac{v_\parallel^2}{v_{th\parallel,h}^2} \right) + n_p \left(\pi v_{th\parallel,p}^2 \right)^{-\frac{1}{2}} \exp\left(-\frac{(v_\parallel - v_b)^2}{v_{th\parallel,p}^2} \right) \tag{1}$$

where n_i and $v_{th\|,i}$ ($i = h$ or p) denote the number density and parallel velocity of the i component, and v_b is the bulk velocity of the plateau component. The cold electron component is not considered, because its thermal velocity is much lower than $0.5V_{Ae}$. Since electron plateau components along with chorus waves are typically observed at $\sim 0.5V_{Ae}$ (Chen et al., 2019; Kong et al., 2021; Li et al., 2019; Min et al., 2014), then the v_b is determined by the positive gradient of PSD in the range of 0.4–$0.6V_{Ae}$ (Min et al., 2014). In Event I, $v_b = 0.431V_{Ae}$ in both directions. In Event II, $v_b = 0.547V_{Ae}$ along wave propagation, and $v_b = 0.487V_{Ae}$ opposite to it. We then fit PSDs by choosing seven adjacent data points (blue circles) around v_b, and the fitting results are represented by red lines. The coefficient R^2 can determine the reliability of fitting parameters ($R^2 = 1 -$ SSE/SST, where SSE is the sum of squares of the difference between the original data and fitting values, and SST is the sum of squares of the difference between the original data and their mean), which is close to 1 when the fitting is reliable. In Event I, $n_p/n_0 = 0.0184$ along wave propagation, and $n_p/n_0 = 0.0214$ opposite to it (with the corresponding R^2 of 0.967 and 0.974, respectively). While in Event II, n_p/n_0 equals 0.0007 and 0.0011 in two directions (with $R^2 = 0.981$ and 0.969, respectively). Other fitting parameters that are not considered in this study can be found in Supporting Information S1.

3.2. Statistical Results

Since power gaps are typically observed near the equator, we only select the chorus events at |MLAT| < 5° between $L = 3$–7 over all MLTs by using Van Allen Probes A and B data during the period from October 2012 to December 2013. The events after 2013 haven't been chosen due to the general deficiency of parallel PSD data from the HOPE instrument. The chorus waves are collected in the frequency range of 0.1–$0.8f_{ce}$, and contain either a power gap around $0.5f_{ce}$, or a continuous band across $0.5f_{ce}$. To reduce the effect of background noises, the wave amplitudes are required to be larger than 0.005 nT, and the selected waves have a right-hand polarization ($\varepsilon > 0.7$) and a large polarization ratio ($R_p > 0.9$). Our chorus data set includes both the rising/falling tone and hiss-like emissions without further distinguishing them, because power gaps are a common feature regardless of whether chorus waves chirp or not (Fu et al., 2014; Gao et al., 2019; Li et al., 2019; Teng et al., 2019). Note that those banded chorus waves with obvious harmonic structures are excluded from our study, since they are generated due to the wave-wave coupling (Chen et al., 2017; Gao et al., 2016, 2017). For each chorus event, we fit PSDs in the directions along and opposite to wave propagation, and only keep the events with $R^2 > 0.9$. At last, we obtain 252 banded events, and 98 no-gap events.

The global distribution of the two types of events in the L-MLT plane is shown in Figure 2a, where chorus waves are mainly detected in $L = 4$–6. However, their preferred MLTs are different. The banded events (red circles) typically occur in the midnight and dawn sectors with MLT = 00–07, while no-gap events (blue circles) are mainly in the dawn and morning sectors with MLT = 05–09. The distributions of event number as a function of wave amplitude $\delta B/B_0$ in (b) banded and (c) no-gap events are also shown. The $\delta B/B_0$ is recorded at the time points when the PSD data is selected. Both types of events have a comparable $\delta B/B_0$, which peaks in the range of 10^{-2}–10^{-1} (with $\sim 78\%$ of banded events and $\sim 64\%$ of no-gap events in this range).

The number densities of plateau components n_p/n_0 in the two types of events are further investigated. Figure 2 shows the distributions of banded event numbers in the (d) same and (f) opposite direction of wave propagation, while the distributions associated with no-gap events are shown in Figures 2e and 2g. In both banded and no-gap events, n_p/n_0 is comparable in the two directions, suggesting that the plateau shapes along wave propagation and opposite to it are almost symmetric inside the source region. For banded events, n_p/n_0 covers a wide range from 10^{-5} to 10^{-2}, and peaks around 10^{-3} (with $\sim 60\%$ of the events in the two adjacent bins around 10^{-3}). While, the n_p/n_0 for no-gap events is much smaller, covering 10^{-6}–10^{-3} and concentrating on $\sim 10^{-4}$ (with $\sim 62\%$ of the events in its two adjacent bins). Therefore, the n_p/n_0 in banded events is approximately one order larger than that in no-gap events, indicating that banded events typically have a more pronounced plateau shape in the velocity distributions.

Chorus waves can interact with plateau components in the same direction through Landau resonance, or with those in the opposite direction through cyclotron resonance. To distinguish the effects of plateau components in different directions, we calculate the linear growth rate via (a) Landau resonance γ_L and (b) cyclotron resonance γ_c in Figure 3, following the method in Brinca (1972). The growth rates for each banded event with a WNA of θ_{avg} (where θ_{avg} is the averaged WNA in the frequency range of 0.1–$0.8f_{ce}$) are denoted by gray lines, and the black lines represent the median values over all events. As shown in Figure 3a, the effect of Landau resonance is quite
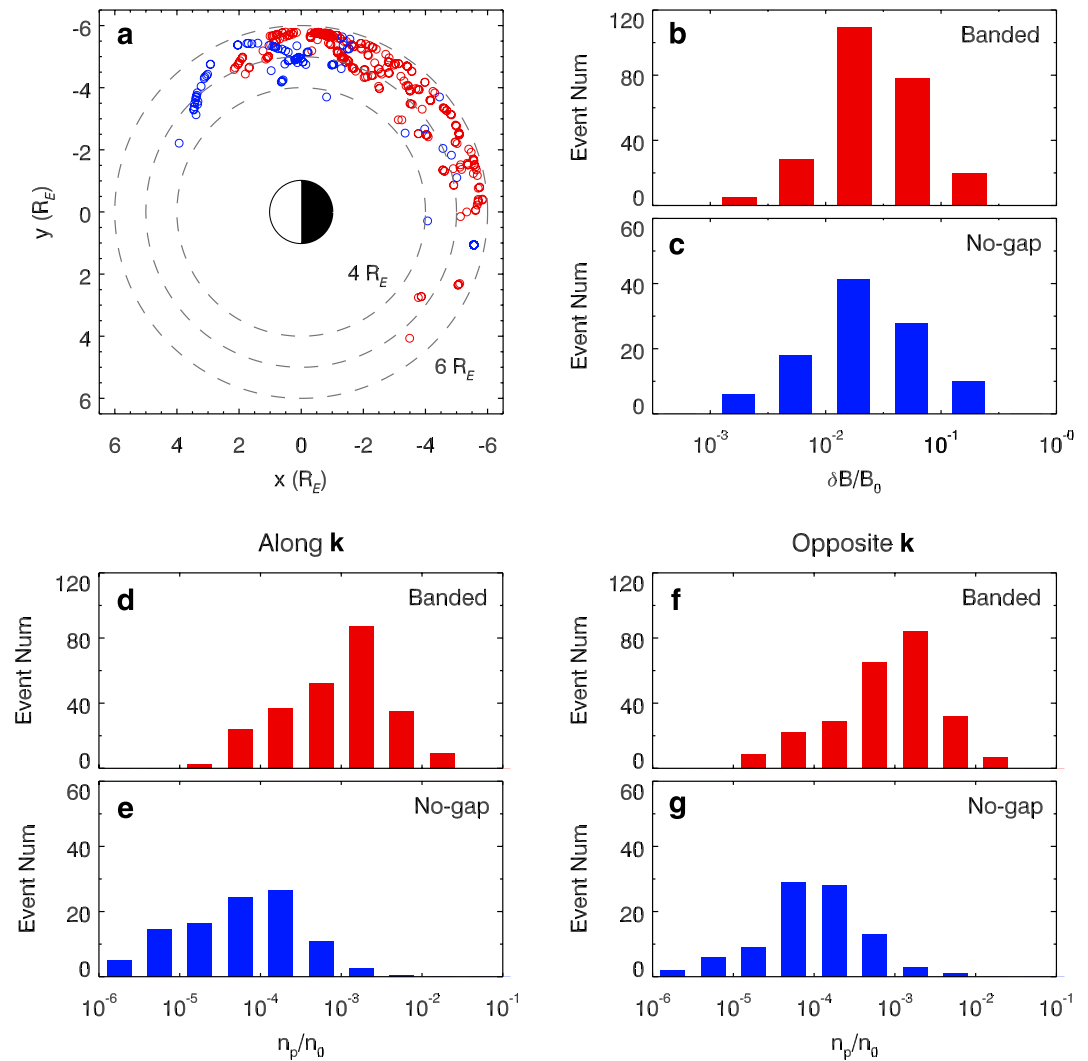
Figure 2. (a) The global distribution of banded (red circles) and no-gap events (blue circles) in the L-MLT plane. The distribution of event numbers as a function of $\delta B/B_0$ in (b) banded and (c) no-gap events. The distribution of event numbers as a function of n_p/n_0 (d, e) along and (f, g) opposite to wave propagation. The top row is for banded events, and the bottom row is for no-gap events.
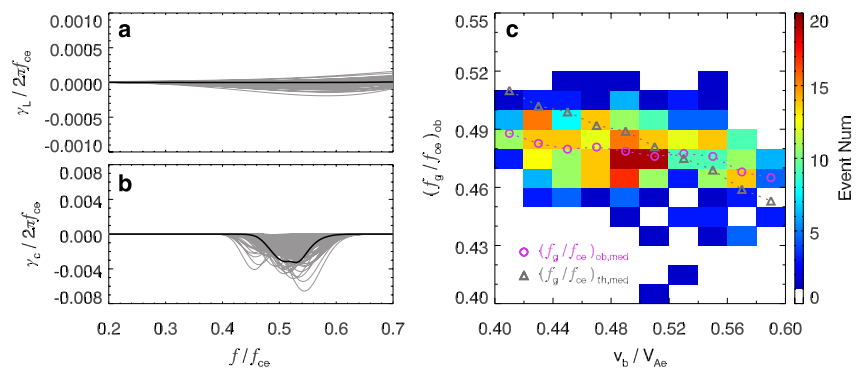

Figure 3. The growth rate via (a) Landau resonance γ_L and (b) cyclotron resonance γ_c as a function of f/f_{ce} for banded events. The gray lines denote the growth rate in each event, and black lines represent median values over all events. The distribution
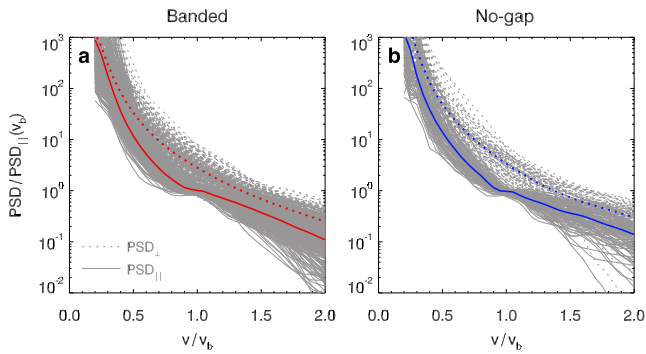
Figure 4. The normalized phase space densities (PSDs) as a function of v/v_b in (a) banded and (b) no-gap events, where the solid and dashed lines represent the parallel and perpendicular PSDs. The gray lines denote PSDs in each event, and the red or blue lines represent the median values.

weak, with a median growth rate of $\gamma_L \approx 0$. While the cyclotron resonance has a significant influence on waves by causing severe damping at $\sim 0.5 f_{ce}$ (with a damping rate of $\sim 10^{-3}$ in Figure 3b), leading to gap formation.

According to the cyclotron resonance condition:

$$2\pi f_g - k_g v_b \cos\theta_g = 2\pi f_{ce} \qquad (2)$$

where k_g and θ_g are the wave number and WNA of chorus waves at $0.5 f_{ce}$, there is an inverse correlation between the gap frequency f_g and the absolute value of the bulk velocity v_b. We further investigate the correlation between v_b and f_g in data. Figure 3c shows the distribution of numbers of banded events in the $v_b - (f_g/f_{ce})_{ob}$ plane, where $(f_g/f_{ce})_{ob}$ is the frequency of the power minimum between two bands in observations. As shown in this figure, $(f_g/f_{ce})_{ob}$ is mainly in the range of 0.46–0.50, while the v_b/V_{Ae} is in a range from 0.42 to 0.58 but clusters in 0.48–0.52. There are also two events have a quite small $(f_g/f_{ce})_{ob}$ (<0.42), but their amplitudes are weak ($\delta B/B_0 \sim 10^{-3}$). In each event, we define the theoretical gap frequency $(f_g/f_{ce})_{th}$ as the frequency with the largest damping rate via cyclotron resonance (Figure 3b). The magenta circles and the gray triangles represent the median values of observed gap frequencies $(f_g/f_{ce})_{ob,med}$ and theoretical gap frequencies $(f_g/f_{ce})_{th,med}$, respectively. It is clearly shown that both $(f_g/f_{ce})_{ob,med}$ and $(f_g/f_{ce})_{th,med}$ are negatively correlated with v_b/V_{Ae}. Moreover, the two frequencies are roughly consistent, further supporting that power gaps are formed due to the cyclotron resonance. However, they still have some differences, which can be related to the rough estimation of WNAs. In the theoretical analysis, we choose the average θ_{avg} rather than the θ_g around $0.5 f_{ce}$, because the θ_g cannot be given accurately from observations due to the weak wave power here.

We further compare the velocity distributions in (a) banded and (b) no-gap events in Figure 4, where the normalized PSDs as a function of v/v_b are shown. Here, the perpendicular PSD (PSD$_\perp$, marked by dashed lines) and the parallel PSD (PSD$_\parallel$, marked by solid lines) are separately considered, and both are normalized to the PSD$_\parallel$ at v_b. Since the PSDs along and opposite to wave propagation are symmetric (Min et al., 2014), we might as well use the PSD along propagation as PSD$_\parallel$. The gray lines represent the distributions in each event, and the red (blue) lines denote the median values over all banded (no-gap) events. In banded events, PSD$_\perp$ is generally larger than PSD$_\parallel$. Although the temperature anisotropy gets somewhat smaller at $\sim 0.5 V_{Ae}$ due to the existence of the plateau shape, it doesn't separate the electron distribution into two distinct components. Moreover, the morphology of the distributions in no-gap events is similar to those in banded events, and they have the comparable temperature anisotropy.

4. Conclusions and Discussion

Based on a survey of over one-year Van Allen Probes data, we have thoroughly investigated both banded and no-gap chorus events, and their correlations with the electron plateau distributions. We find that the banded events are primarily in the midnight and dawn sectors, while no-gap events predominantly occur in the dawn and morning sectors. In both types of events, obvious plateau components are forming at $\sim 0.5 V_{Ae}$ in the parallel velocity distributions. However, banded events usually have a much larger number density of plateau components ($n_p/n_0 \sim 10^{-3}$) than no-gap events ($\sim 10^{-4}$). The plateau components can cause severe damping at $\sim 0.5 f_{ce}$ via cyclotron resonance rather than Landau resonance. Moreover, the gap frequencies given by the cyclotron resonant condition are roughly consistent with those in observations, providing observational evidence that the power gaps can be produced due to the cyclotron resonance. Last but not least, we also find that there is no significant difference between the normalized velocity distributions in banded and no-gap events.

By analyzing several banded events in observations, Li et al. (2019) have suggested that the plateau components can divide the electrons into two populations, which then separately excite upper band and lower band waves, leaving a gap between them. This suggests that the velocity distributions in banded and no-gap events should be quite different. However, we find that the difference in the normalized velocity distributions between the two types of events is not significant. Moreover, it is difficult to pick out two distinct components from the entire electron velocity distribution (Figure 4). This indicates that the mechanism in Li et al. (2019) cannot be well

supported by the present velocity distributions. However, this mechanism may still take effect in the events where n_p/n_0 is quite large and the two distinct components are formed. By calculating the energy transfer between chorus waves and electrons via Landau resonance, Hsieh and Omura (2018) have shown that the damping in the lower latitudes ($\lambda < 5°$) is typical quite weaker than that in the higher latitudes. Since the banded events in our study are all near the equator, the nonlinear damping via Landau resonance can be ignored. Nevertheless, it is not excluded that the nonlinear damping mechanism can account for the banded events in relatively higher latitudes. The rough consistency between the f_g in observation and given by the cyclotron resonance condition seems to support the "spectrum bite" mechanism.

By performing particle-in-cell simulations, Chen, Gao, et al. (2022) have found that the plateau components at $\sim 0.5V_{Ae}$ can be self-consistently generated by non-parallel chorus waves via Landau resonance. Their number densities are estimated as $n_p/n_0 \sim 10^{-3}$, consistent with those in banded chorus events from observations (Figures 2d and 2f). In the magnetosphere, the plateau components are commonly observed along with chorus waves (Chen et al., 2019; Kong et al., 2021; Li et al., 2019; Li, Mourenas, et al., 2016; Min et al., 2014). With THEMIS data, Min et al. (2014) have suggested that the bulk velocities of plateau components generally match the Landau resonant velocities of chorus waves, indicating these components are formed due to Landau resonance. This is further supported by Chen et al. (2019), which have found that n_p/n_0 is positively correlated with the wave parallel electric field. In this study, plateau components can be generated through the Landau resonance by chorus waves, due to the consistency of n_p/n_0 with those in the simulations (Chen, Gao, et al., 2022). However, Artemyev and Mourenas (2020) have suggested that the kinetic Alfven wave or time domain structure can also produce the plateau components, which cannot be excluded from our study.

Our observations reveal that the no-gap events preferentially occur on the dayside, unlike banded events mainly on the nightside (Figure 2a), which is consistent with Teng et al. (2019). This day-night asymmetry can be explained based on the "spectrum bite" mechanism. The magnetic fields on the dayside are more flattened due to the solar wind pressure. The waves propagate almost along the field lines, so the Landau resonance is quite weak, which ultimately causes the negligible plateau components in no-gap events. Our study provides a more comprehensive understanding of how the evolution of electron distribution affects chorus waves.

Data Availability Statement

All the data from Van Allen Probes were from https://spdf.gsfc.nasa.gov/pub/data/rbsp/.

References

Artemyev, A. V., & Mourenas, D. (2020). On whistler mode wave relation to electron field-aligned plateau populations. *Journal of Geophysical Research: Space Physics*, *125*(3), e2019JA027735. https://doi.org/10.1029/2019JA027735

Brinca, A. L. (1972). On the stability of obliquely propagating whistlers. *Journal of Geophysical Research*, *77*(19), 3495–3507. https://doi.org/10.1029/JA077i019p03495

Burtis, W. J., & Helliwell, R. A. (1969). Banded chorus a new type of VLF radiation observed in the magnetosphere by OGO 1 and OGO 3. *Journal of Geophysical Research*, *74*(11), 3002–3010. https://doi.org/10.1029/ja074i011p03002

Chen, H., Gao, X., Lu, Q., Fan, K., Ke, Y., Wang, X., & Wang, S. (2022). Gap formation around $0.5\Omega_e$ in the whistler mode waves due to the plateau-like shape in the parallel electron distribution: 2D PIC simulations. *Journal of Geophysical Research: Space Physics*, *127*(5), e2021JA030119. https://doi.org/10.1029/2021JA030119

Chen, H., Gao, X., Lu, Q., Ke, Y., & Wang, S. (2017). Lower band cascade of whistler waves excited by anisotropic hot electrons: One-dimensional PIC simulations. *Journal of Geophysical Research: Space Physics*, *122*(10), 10448–10457. https://doi.org/10.1002/2017JA024513

Chen, H., Gao, X., Lu, Q., Sauer, K., Chen, R., Yao, J., & Wang, S. (2021). Gap formation around $0.5\Omega_e$ of whistler-mode waves excited by electron temperature anisotropy. *Journal of Geophysical Research: Space Physics*, *126*(2), e2020JA028631. https://doi.org/10.1029/2020JA028631

Chen, H., Lu, Q., Wang, X., Fan, K., Chen, R., & Gao, X. (2022). One-dimensional gcPIC-δf simulation of hooked chorus waves in the Earth's inner magnetosphere. *Geophysical Research Letters*, *49*(4), e2022GL097989. https://doi.org/10.1029/2022GL097989

Chen, R., Gao, X., Lu, Q., & Wang, S. (2019). Unraveling the correlation between chorus wave and electron beam-like distribution in the Earth's magnetosphere. *Geophysical Research Letters*, *46*(21), 11671–11678. https://doi.org/10.1029/2019GL085108

Fu, X., Cowee, M. M., Friedel, R. H., Funsten, H. O., Gary, S. P., Hospodarsky, G. B., et al. (2014). Whistler anisotropy instabilities as the source of banded chorus: Van Allen Probes observations and particle-in-cell simulations. *Journal of Geophysical Research: Space Physics*, *119*(10), 8288–8298. https://doi.org/10.1002/2014JA020364

Funsten, H. O., Skoug, R. M., Guthrie, A. A., MacDonald, E. A., Baldonado, J. R., Harper, R. W., et al. (2013). Helium, Oxygen, Proton, and Electron (HOPE) mass spectrometer for the radiation belt storm probes mission. *Space Science Reviews*, *179*, 423–484. https://doi.org/10.1007/978-1-4899-7433-4_13

Gao, X., Chen, L., Li, W., Lu, Q., & Wang, S. (2019). Statistical results of the power gap between lower-band and upper-band chorus waves. *Geophysical Research Letters*, *46*(8), 4098–4105. https://doi.org/10.1029/2019GL082140

Gao, X., Chen, R., Lu, Q., Chen, L., Chen, H., & Wang, X. (2022). Observational evidence for the origin of repetitive chorus emissions. *Geophysical Research Letters*, *49*(12), e2022GL099000. https://doi.org/10.1029/2022GL099000

Gao, X. L., Ke, Y. G., Lu, Q. M., Chen, L. J., & Wang, S. (2017). Generation of multiband chorus in the Earth's magnetosphere: 1-D PIC simulation. *Geophysical Research Letters*, *44*(2), 618–624. https://doi.org/10.1002/2016GL072251

Gao, X. L., Lu, Q. M., Bortnik, J., Li, W., Chen, L. J., & Wang, S. (2016). Generation of multiband chorus by lower band cascade in the Earth's magnetosphere. *Geophysical Research Letters*, *43*(6), 2343–2350. https://doi.org/10.1002/2016GL068313

Horne, R. B., & Thorne, R. M. (1998). Potential waves for relativistic electron scattering and stochastic acceleration during magnetic storms. *Geophysical Research Letters*, *25*(15), 3011–3014. https://doi.org/10.1029/98GL01002

Hsieh, Y.-K., & Omura, Y. (2018). Nonlinear damping of oblique whistler mode waves via Landau resonance. *Journal of Geophysical Research: Space Physics*, *123*(9), 7462–7472. https://doi.org/10.1029/2018JA025848

Kasahara, S., Miyoshi, Y., Yokota, S., Mitani, T., Kasahara, Y., Matsuda, S., et al. (2018). Pulsating aurora from electron scattering by chorus waves. *Nature*, *554*(7692), 337–340. https://doi.org/10.1038/nature25505

Kessel, R. L., Fox, N. J., & Weiss, M. (2012). The radiation belt storm probes (RBSP) and space weather. *Space Science Reviews*, *179*(1–4), 531–543. https://doi.org/10.1007/s11214-012-9953-6

Kletzing, C. A., Kurth, W. S., Acuna, M., MacDowall, R. J., Torbert, R. B., Averkamp, T., et al. (2013). The electric and magnetic field instrument suite and integrated science (EMFISIS) on RBSP. *Space Science Reviews*, *179*(1-4), 127–181. https://doi.org/10.1007/s11214-013-9993-6

Kong, Z., Gao, X., Chen, H., Lu, Q., Chen, R., Ke, Y., & Wang, S. (2021). The correlation between whistler mode waves and electron beam-like distribution: Test particle simulations and THEMIS observations. *Journal of Geophysical Research: Space Physics*, *126*(11), e2021JA029834. https://doi.org/10.1029/2021JA029834

Kurth, W. S., De Pascuale, S., Faden, J. B., Kletzing, C. A., Hospodarsky, G. B., Thaller, S., & Wygant, J. R. (2015). Electron densities inferred from plasma wave spectra obtained by the Waves instrument on Van Allen Probes. *Journal of Geophysical Research: Space Physics*, *120*(2), 904–914. https://doi.org/10.1002/2014JA020857

Li, J., Bortnik, J., An, X., Li, W., Angelopoulos, V., Thorne, R. M., et al. (2019). Origin of two-band chorus in the radiation belt of Earth. *Nature Communications*, *10*(1), 4672. https://doi.org/10.1038/s41467-019-12561-3

Li, W., Bortnik, J., Thorne, R. M., & Angelopoulos, V. (2011). Global distribution of wave amplitudes and wave normal angles of chorus waves using THEMIS wave observations. *Journal of Geophysical Research*, *116*(A12), A12205. https://doi.org/10.1029/2011JA017035

Li, W., Mourenas, D., Artemyev, A. V., Bortnik, J., Thorne, R. M., Kletzing, C. A., et al. (2016). Unraveling the excitation mechanisms of highly oblique lower band chorus waves. *Geophysical Research Letters*, *43*(17), 8867–8875. https://doi.org/10.1002/2016GL070386

Liu, K., Gary, S. P., & Winske, D. (2011). Excitation of banded whistler waves in the magnetosphere. *Geophysical Research Letters*, *38*(14), L14108. https://doi.org/10.1029/2011GL048375

Lu, Q., Chen, L., Wang, X., Gao, X., Lin, Y., & Wang, S. (2021). Repetitive emissions of rising-tone chorus waves in the inner magnetosphere. *Geophysical Research Letters*, *48*(15), e2021GL094979. https://doi.org/10.1029/2021GL094979

Meredith, N. P., Horne, R. B., & Anderson, R. R. (2001). Substorm dependence of chorus amplitudes: Implications for the acceleration of electrons to relativistic energies. *Journal of Geophysical Research*, *106*(A7), 13165–13178. https://doi.org/10.1029/2000JA900156

Min, K., Liu, K., & Li, W. (2014). Signatures of electron Landau resonant interactions with chorus waves from THEMIS observations. *Journal of Geophysical Research: Space Physics*, *119*(7), 5551–5560. https://doi.org/10.1002/2014JA019903

Nishimura, Y., Bortnik, J., Li, W., Thorne, R. M., Ni, B., Lyons, L. R., et al. (2013). Structures of dayside whistler-mode waves deduced from conjugate diffuse aurora. *Journal of Geophysical Research: Space Physics*, *118*(2), 664–673. https://doi.org/10.1029/2012ja018242

Omura, Y., Hikishima, M., Katoh, Y., Summers, D., & Yagitani, S. (2009). Nonlinear mechanisms of lower-band and upper-band VLF chorus emissions in the magnetosphere. *Journal of Geophysical Research*, *114*(A7), A07217. https://doi.org/10.1029/2009JA014206

Summers, D., Thorne, R. M., & Xiao, F. L. (1998). Relativistic theory of wave-particle resonant diffusion with application to electron acceleration in the magnetosphere. *Journal of Geophysical Research*, *103*(A9), 20487–20500. https://doi.org/10.1029/98JA01740

Teng, S., Tao, X., & Li, W. (2019). Typical characteristics of whistler mode waves categorized by their spectral properties using Van Allen Probes observations. *Geophysical Research Letters*, *46*(7), 3607–3614. https://doi.org/10.1029/2019GL082161

Thorne, R. M., Li, W., Ni, B., Ma, Q., Bortnik, J., Chen, L., et al. (2013). Rapid local acceleration of relativistic radiation-belt electrons by magnetospheric chorus. *Nature*, *504*(7480), 411–414. https://doi.org/10.1038/nature12889

Tsurutani, B. T., & Smith, E. J. (1974). Postmidnight chorus: A substorm phenomenon. *Journal of Geophysical Research*, *79*(1), 118–127. https://doi.org/10.1029/JA079i001p00118

Tsurutani, B. T., & Smith, E. J. (1977). Two types of magnetospheric ELF chorus and their substorm dependences. *Journal of Geophysical Research*, *82*(32), 5112–5128. https://doi.org/10.1029/JA082i032p05112